Nuclear Engineering and Technology 53 (2021) 3580–3596

Contents lists available at ScienceDirect

Nuclear Engineering and Technology

journal homepage: www.elsevier.com/locate/net

Original Article

PILLAR: Integral test facility for LBE-cooled passive small modular reactor research and computational code benchmark

Yong-Hoon Shin [a], Jaeyeong Park [b, *], Jungho Hur [b], Seongjin Jeong [a], Il Soon Hwang [a]

[a] Department of Energy Systems Engineering, Seoul National University, 1 Gwanak-ro, Gwanak-gu, Seoul, 08826, Republic of Korea
[b] School of Mechanical, Aerospace and Nuclear Engineering, Ulsan National Institute of Science and Technology, Ulju-gun, Ulsan, 44919, Republic of Korea

ARTICLE INFO

Article history:
Received 20 March 2021
Received in revised form
13 May 2021
Accepted 17 May 2021
Available online 22 May 2021

Keywords:
Integral test facility
Small modular reactor
Lead-bismuth eutectic
Natural circulation
Thermal-hydraulic scale experiment
System code benchmark

ABSTRACT

An integral test facility, PILLAR, was commissioned, aiming to provide valuable experimental results which can be referenced by system and component designers and used for the performance demonstration of liquid-metal-cooled, passive small modular reactors (SMRs) toward their licensing. The setup was conceptualized by a scaling analysis which allows the vertical arrangements to be conserved from its prototypic reactor, scaled uniformly in the radial direction achieving a flow area reduction of 1/200. Its final design includes several heater rods which simulate the reactor core, and a single heat exchanger representing the steam generators in the prototype. The system behaviors were characterized by its data acquisition system implementing various instruments. In this paper, we present not only a detailed description of the facility components, but also selected experimental results of both steady-state and transient cases. The obtained steady-state test results were utilized for the benchmark of a system code, achieving a capability of accurate simulations with ±3% of maximum deviations. It was followed by qualitative comparisons on the transient test results which indicate that the integral system behaviors in passive LBE-cooled systems are able to be predicted by the code.

1. Introduction

Small modular reactors (SMRs) are generally defined as nuclear power plants which have nominal power ratings lower than or equal to 300 MW_e [1] and are modularized so that factory fabrication is viable. Their strengths over large-scale nuclear power reactors can be justified from an economic perspective: the financial risk of initial investment can be reduced thanks to their reduced power outputs and size [2]. In addition, SMRs are more competitive than those large reactors when deployed to remote areas where no power grid exists and to microgrids where electricity is generated and distributed in a small region isolated from the main grid [3]. An optimistic prospect suggests up to 21 GW of the world's electricity consumption could be supported by SMRs by 2035 [4], which is reasonable considering the fact that more than 70 SMR conceptual designs are under development [1].

Even though water-cooled SMRs are evaluated to be deployed in the nearest term as their technology readiness levels are higher with an accumulated experience with the Generation-II and III reactors, some adopt lead or lead-bismuth eutectic (LBE) as primary coolants, motivated by their promising features for a significant enhancement in inherent safety. Chemical inertness is the key consideration, as it excludes the possibility of thermal and pressure load from hydrogen explosion in water reactors or sodium fire in sodium reactors. High boiling points (2021 K for lead, 1943 K for LBE) enable a system to be free of pressurization and contribute to avoiding the risk of coolant boiling. Besides, considerably high thermal conductivity (16.6 W/m K for lead at 673 K and 11.8 W/m K for LBE at 573 K) allows a system to be cooled effectively even under adverse circumstances. A high retention capability for radionuclides makes the heavy liquid metal coolants work as an additional engineered barrier [5]. An outstanding safety and system simplification can also be realized by excluding the primary pumps by design and through natural circulation of the heavy liquid metals. In particular, lead and LBE allows a significantly reduced pressure loss in the core, which takes up most of the hydraulic loss along the flow path, by increasing the pin pitch and thus free flow area in the fuel bundle [6].

In this regard, several SMR designs based on the heavy liquid metal coolants have been developed and suggested to make use of those advantages. Hydromine is developing a compact lead-cooled

* Corresponding author.
E-mail address: jypark@unist.ac.kr (J. Park).

https://doi.org/10.1016/j.net.2021.05.024

Nomenclature

a	Flow area (m^2)
A	Nondimensional flow area normalized by the reference flow area
Bi	Biot number
C_p	Isobaric heat capacity (J/kg K)
d	Hydraulic diameter (m)
d_{rod}	Diameter of nuclear fuel rod or electrical heater rod (m)
f	Darcy-Weisbach friction factor
F	Friction number
g	Gravitational acceleration constant (m/s^2)
h	Convective heat transfer coefficient (W/m^2 K)
k	Conductive thermal conductivity (W/m K)
K	Form loss coefficient
l	Length of a component (m)
L	Nondimensional length
$\dot{m}$	Mass flow rate (kg/s)
N_{rod}	Number of nuclear fuel rods or electrical heater rods
Nu	Nusselt number
P_0	Core thermal power (W)
Pe	Peclet number
Pr	Prandtl number
$\dot{q}$	Volumetric heat generation rate (W/m^3)
Q	Heat source number
Re	Reynolds number
Ri	Richardson number
St	Stanton number
t	Time (s)
T	Temperature (K)
Ti	Time ratio number
u	Area-averaged flow velocity (m/s)
U	Nondimensional flow velocity
y	Transverse distance to flow direction (m)
Y	Nondimensional transverse distance
z	Vertical (flow direction) distance (m)
Z	Nondimensional axial distance

Greek letters

α	Thermal diffusivity (m^2/s)
β	Thermal coefficient of expansion (K^{-1})
δ	Conduction depth (m)
θ	Nondimensional temperature difference
ξ	Wetted perimeter (m)
ρ	Density (kg/m^3)
τ	Nondimensional time
ψ	Specific parameter

Subscripts

0	Reference
c	Cold region
h	Hot region
i	Component number
m	Scale model
p	Prototype
r	Representative variable of system
R	Model-to-prototype ratio such that $\psi_R = \psi_m/\psi_p$
s	Solid

SMR, LFR-AS-200, which features a nominal power output of 200 MW_e and the primary system being arranged in a single reactor pool [7]. SEALER aims at being deployed to remote communities and mining sites in the Canadian Arctic [8]. Loading 19.9%-enriched UO_2 fuel, this reactor can vary its electricity production in a range of 3–10 MW while the lifetime of the core varies between 10 and 30 full power years with 90% capacity factor. G4M, also known as Hyperion, has a power capacity of 70 MW_{th}, around 25 MW_e per unit [9]. Its three potential applications were identified as mining areas, remote communities, and government facilities. A Russian design of SVBR-75/100 can serve multiple purposes such as replacing old NPP units, supplying heat and electricity close to urban areas, desalinating seawater in developing countries with its relatively small power rating within a single module [10]. In addition, its versatile fuel loading strategy implements different types of nuclear fuel such as UO_2, mixed oxide, and mixed nitride fuels. The deployment of SMRs all around the globe may bring up a nuclear proliferation concern. PASCAR and URANUS fully exploit a single fuel cycle up to 20 years without on-site refueling indicating that such concern can be overcome by sophisticated designs [11,12]. These SMRs also achieve an enhanced inherent safety in conjunction with their streamlined designs relying solely on natural circulation during normal operation and under accidental conditions.

For a successful development and deployment of SMRs, it can be rationalized that dedicated test setups for SMR research should be prepared and commissioned. The most distinct feature of SMRs from large-scale reactors is their compact designs satisfying certain dimensional limits. Furthermore, several designs aim to exclude the use of reactor coolant pump in the primary system. These design features might lead to difficulty in assessment of their thermal-hydraulic behaviors by using conventional computation tools which have been developed for loop-type, active systems.

However, almost little attention has been paid to the integral test facility for lead- or LBE-cooled SMRs in contrast to the fact that several test setups for water-cooled SMRs have been reported. To name a few, the NuScale Power has operated the NIST facility together with its consortium, which is a 1/3-scale model in height while preserving the prototypic reactor's key operating conditions such as pressure and temperature [13]. Its main objectives are to validate the performance of its emergency core cooling system and long-term cooling capabilities. VISTA-ITL is a scaled integral test facility of the SMART reactor developed by KAERI, which focuses on the performance verification of passive safety functions and validation of system codes [14].

To fill the gap in the experimental capability on heavy liquid metal cooled SMR research and development, we designed and commissioned an integral experimental facility PILLAR (Pool-type Integral Leading test facility for Lead-Alloy-cooled small modular Reactor research) through a comprehensive review on a number of scaling analysis methods that can be applied to passive liquid metal systems. The URANUS reactor [12] was selected to be the prototype of the facility from which the scaling was made. PILLAR features the conservation of scale in the vertical direction while its radial dimensions are reduced proportionally with a factor of ca. 1/14, allowing some geometrical adaptations. Several natural circulation test runs including a number of steady-state and transient cases were carried out. The former cases were defined by the total power rating given to the core simulator and reported with mean values averaged over at least a time period longer than 2 h. On the other hands, the transient tests were initiated by perturbations in the core power and water side flow rate and were monitored for around 1 h. Furthermore, a one-dimensional system code was

benchmarked with the steady-state test results, while its simulation capability was extended and evaluated qualitatively on the transient test results.

2. Design approach

2.1. Scaling methods for passive liquid metal cooled reactors

So far, a number of scaling methods have been suggested to be applied to real-world experiments. Of many scaling methods developed, this section summarizes those applicable for liquid metal cooled fast reactors and selects the most valid method for the scaling design of the integral test facility.

In 1982, a scaling method on natural circulation in sodium-cooled fast reactors (SFR) was suggested to be tested with water as its density is comparable to that of sodium [15]. However, the paper did not clearly articulate how the representative velocity and the representative temperature difference are derived from governing equations, nor how a parameter called Euler number works. In addition, the authors simply proposed a possibility that an experimental facility with water could simulate thermal-hydraulic behaviors cast in SFRs if similarities in main dimensionless numbers are met. Similarly, a method to experimentally simulate decay heat removal in SFRs with water was proposed in the early 1990s [16]. In this study, two main parameters, the representative velocity and representative temperature difference, were fixed to the core outlet velocity and core inlet-outlet temperature difference, respectively.

Scaling methods on pool-type SFRs were reported as well [17,18], which originally aimed at facilitating water in experimental facilities instead of sodium since the optical transparency and material compatibility of water ensure a simpler and safer operation. The method features that the geometrical similitudes in all directions are equal so that a scale model is able to be reduced without any distortion in a specific direction from a prototype. In addition, heat source and heat sink are regarded as “black boxes” which allow such parts to be designed arbitrarily in their shapes. Internal flow directions in these black boxes are supposed to be unidirectional. Furthermore, this study covered the role of Euler number in scaling analysis and the necessity of its conservation, which were not fully explained by the previous studies. Recently, this method was applied to the design of E-SCAPE, a scale model of MYRRHA [19]. It is noted that both the prototype and the scale facility adopted LBE as their primary coolant.

Likewise, a study proposed simulating a pool-type passive LFR with water [20]; in addition, a methodology evaluating the stability of natural circulation flow in the water model. However, a test facility designed through this method would require water temperature to be maintained higher than its boiling point, leading to a necessity of proper pressurization means.

A scaling method through area-averaged one-dimensional formulations was developed, which can be applied to both single-phase and two-phase flows [21,22]. This method employs a set of governing equations including conservation in mass, momentum, and energy in solid and fluid domains, and additionally a closure relation for a boundary condition between the solid and fluid domains. These one-dimensional formulations are non-dimensionalized by a steady-state solution, especially the representative velocity and representative temperature difference. This method features that the scaling ratio in the lateral direction perpendicular to the flow direction is able to be decided independently and heat transfer between solid heat sources and the fluid is considered so that the similarity in transient conditions is also conserved. On the other hand, it has a limitation in simulating local phenomena as any radial dependence is neglected in the governing equations by averaging parameters over the flow area. Although the method was originally developed for water, it is applicable to a liquid metal as long as its thermophysical properties are relatively constant over a moderate temperature range.

2.2. Design requirements and determination of scaling method

Prior to the selection of scaling method, the design requirements of PILLAR were identified. As the driving force of natural circulation is strongly coupled with the height difference between heat sink and heat source, the length scale in the vertical direction was designated to be unity between the prototype and the model to minimize any distortion from integral behaviors. As a result, the flow area was reduced instead, with respect to its volume reduction, and simultaneously, it was necessary that the thickness of each physical component was in compliance with a design pressure of 20 bar. An additional requirement was imposed on the mean velocity at the core outlet, which is the reference velocity on the scaling analysis, to be greater than 10 cm/s so that flow measurement is viable. Lastly, the scale facility shall adopt LBE as working fluid so its capability of natural circulation is able to be directly validated. The requirements and consideration taken are summarized in Table 1.

Among the available methods reviewed in Section 2.1, the scaling method on which the PILLAR design was based was determined in consideration of those requirements. First of all, the scaling methods suggested in Refs. [15,16] were excluded since their applications have almost not been reported. As the height scale was to be preserved, those for the geometrical scaling in all directions [17,18] were ruled out in spite of some applications. The method suggested by Ref. [20] was not applicable as the working fluid should be kept to be LBE.

Hence, the scaling ratios in the longitudinal directions needed to be differentiated from that in the vertical direction to meet the height scale requirements which leads to the application of area-average method [21,22]. It can also be applied to liquid metal environments as shown in the cases of HELIOS and STELLA-1 [23,24]. Furthermore, as the method is not valid for local phenomena to be undistorted, the facility aims to enable integral testing which can support the verification of global behaviors.

3. Scaling design

3.1. Similarity requirements and scaling analysis

The similarity requirements of PILLAR from URANUS were determined based on the scaling analysis by Ref. [21], which features six nondimensional parameters as summed up in Table 2 (see the original article for the full derivation). Besides, the following assumptions are accompanied:

1) the working fluid is incompressible and its density change over the operational temperature range is linear so that the Boussinesq approximation is applied the buoyancy term;

Table 1
PILLAR design requirements and criteria for scaling analysis.

Criterion	Facility limitation/requirement
Length scale	1:1
Flow area scale	Limited by the total amount of LBE (<1/100)
Total LBE mass	<4.0 ton
Core outlet flow velocity	>10 cm/s
Design pressure	20 bar (2.0 MPa)

Table 2
Definition and physical meaning of nondimensional numbers.

Nondimensional number	Formula	Physical meaning
Richardson number	$\mathrm{Ri}\equiv\frac{g\beta\Delta T_0 l_0}{{u_0}^2}$	Ratio of buoyancy to inertia
Friction number	$F_i\equiv\left(\frac{l}{d}f+K\right)_i$	Ratio of friction to inertia
(Modified) Stanton number	$\mathrm{St}_i\equiv\left(\frac{4hl_0}{\rho C_p u_0 d}\right)_i$	Ratio of convective heat transfer from solid heat source wall to fluid to convective heat transfer in flow direction
Time ratio number	$\mathrm{Ti}_i\equiv\left(\frac{\alpha_s}{\delta^2}\frac{l_0}{u_0}\right)_i$	Ratio of transport time to conduction time
Biot number	$\mathrm{Bi}_i\equiv\left(\frac{h\delta}{k_s}\right)_i$	Ratio of convective heat transfer from solid heat source wall to fluid to thermal conductivity in solid heat source
Heat source number	$Q_{si}\equiv\left(\frac{\dot{q}_s l_0}{\rho_s C_{ps} u_0 \Delta T_0}\right)_i$	Ratio of heat source output to energy transfer rate in the flow direction

2) the thermophysical properties of the working fluid are isotropic and constant to temperature change; and
3) heat generated in a solid heat source only conducts in the radial direction while heat conduction in the working fluid along the flow direction is neglected.

The nondimensional formulations are built up by geometrical, dynamic, and kinematic similarities. Firstly, the geometrical similarity is the most fundamental criterion and defined as the dimensionless area ratio and dimensionless length ratio, respectively,

$$A_{iR}=\frac{A_{im}}{A_{ip}}=\frac{(a_i/a_0)_m}{(a_i/a_0)_p}=1, \text{and} \tag{1}$$

$$L_{iR}=\frac{(l_i/l_0)_m}{(l_i/l_0)_p}=1 \quad \left(L_{hR}=\frac{(l_h/l_0)_m}{(l_h/l_0)_p}=1\right). \tag{2}$$

In this study, the core, which drives overall behaviors of the system as a heat source and determines natural circulation flow rate, is forced to be in geometrical similarity while a slight geometrical distortion on other components is tolerated. Furthermore, L_{hR}, which describes the height difference between heat source and heat sink, is strictly conserved.

From the dynamic similarity, the following relation (3) is established

$$\left(\sum_i F_i \Big/ {A_i}^2\right)_R=1. \tag{3}$$

The similarity in pressure drop is difficult to be kept as the total pressure loss tends to reduce more than needed with the geometrical scale reduction. Instead, the criterion can be met by adding some parts that can provide an additional hydraulic loss such as an orifice.

The kinematic similarity should be conserved regardless of other parameters. As assumed that the thermophysical properties of the working fluid are constant over the relevant temperature range, the ratios between the prototype and the model of those are imposed to be unity ($\rho_R = C_{pR} = \beta_R \sim 1$). This further simplifies the ratio of each similarity group given in Table 2 as

$$\mathrm{Ri}_R=\frac{\Delta T_{0R} l_{0R}}{u_{0R}^2}, \tag{4}$$

$$\mathrm{St}_{iR}=\frac{h_{iR} l_{0R}}{u_{0R} d_{iR}}, \tag{5}$$

$$\mathrm{Bi}_R=\frac{h_{iR}\delta_{iR}}{k_{siR}}, \tag{6}$$

$$\mathrm{Ti}_{iR}=\frac{\alpha_{s_R} l_{0R}}{\delta_{iR}^2 u_{0R}}, \text{and} \tag{7}$$

$$Q_{s0R}=\frac{\dot{q}_{s0R} l_{0R}}{u_{0R}\Delta T_{0R}}. \tag{8}$$

Once a ratio is given to be unity, the relevant phenomenon parametrized by each of the terms is able to be strictly conserved.

The velocity requirement can be independently set if the similarity in Ri_R is ensured; in other words, equation (4) equals unity

$$u_{0R}=\Delta T_{0R}^{1/2} l_{0R}^{1/2}. \tag{9}$$

Consequently, the ratios of Ti, Bi, and St for each component, denoted by Ti_{iR}, Bi_{iR}, and St_{iR}, respectively, give rise to the requirements on δ_{iR}, h_{iR}, and d_{iR}. Through this process, the three parameters can be specified as functions of the ratios of solid thermophysical properties (ρ_s, C_{ps}, k_s, and α_s), l_{0R}, and ΔT_{0R}, provided that all the relevant nondimensional parameters are unity as

$$\delta_{iR}=\left(\frac{\alpha_{sR} l_{0R}}{u_{0R}}\right)^{1/2}=\alpha_{sR}^{1/2} l_{0R}^{1/4}\Delta T_{0R}^{-1/4}, \tag{10}$$

$$h_{iR}=\frac{k_{siR}}{\delta_{iR}}=(k_s\rho_s C_{ps})_{iR}^{1/2} l_{0R}^{-1/4}\Delta T_{0R}^{1/4}, \text{and} \tag{11}$$

$$d_{iR}=\frac{h_{iR} l_{0R}}{u_{0R}}=(k_s\rho_s C_{ps})_{iR}^{1/2} l_{0R}^{1/4}\Delta T_{0R}^{-1/4}. \tag{12}$$

In this situation, if the similarities of Ti_i, Bi_i, and Q_i are conserved, then that of St_i is trivially obtained

$$\mathrm{St}_{iR}=\frac{h_{iR} l_{0R}}{u_{0R} d_{iR}}=\mathrm{Ti}_i\mathrm{Bi}_i\frac{(\rho_s C_{ps})_R \alpha_{s0R}}{a_{0R}}=1. \tag{13}$$

However, the similarity in Bi_i is hard to be met since it is parametrized by h_i [21]. For LBE in turbulent flow regime, Seban-Shimazaki correlation, equation (14), is applied [25].

$$\mathrm{Nu}_{LBE} = 5.0 + 0.025(\mathrm{RePr})^{0.8} = 5.0 + 0.025\mathrm{Pe}^{0.8}. \quad (14)$$

Hereinafter, the flow is always assumed to be turbulent, as LBE density is so large that it tends to have a large Re value. As the prototype and the scale model utilize the same working fluid, Pr is almost the same. On the other hand, Re would differ, indicating that simultaneous conservation in Bi and St is difficult to be achieved. Hence, distortion in those factors is inevitable, which in turn leads to distortion in hydraulic diameter and convective heat transfer coefficient as well.

As the similarity distortion in Bi and St is inevitable, the similarity of nondimensional numbers parametrizing heat transfer should be conserved by securing the similarity of Ti and Q_i. Both nuclear fuel rods in the prototypic reactor and heater rods in the scale facility are cylindrical, which can contribute to the similarity of the two nondimensional numbers. Since both d_{iR} and δ_{iR} are in the length dimensions, $d_{rod,R}$ can be determined by equation (15) from the similarity of Ti_{iR} in equation (7)

$$d_{rod,R} = \delta_{0R} = \alpha_{sR}^{1/2} l_{0R}^{1/4} \Delta T_{0R}^{-1/4}. \quad (15)$$

The requirements on thermal output can be derived as

$$u_{0R} a_{0R} \Delta T_{0R} = \dot{q}_{s0R} a_{s0R} l_{0R} \;\Rightarrow\; a_{0R} = (\rho_s C_{ps})_R a_{s0R}. \quad (16)$$

It suggests that the flow area scale and the cross-sectional area scale of the solid heat source vary with the heat capacity ratio per unit volume when the ratio of the thermophysical properties of heat source differs. It is noted that the original article assumed the solid properties are kept identical between the prototype and the model. Practically, however, it is not possible as nuclear fuel rods have to be simulated by heater rods. Hence, if the ratio of the heat capacity per unit volume is large, the solid heat source area will be reduced more than the flow area, and vice versa. The following Section 3.2 is dedicated for the comparison of such materials.

Finally, the volumetric power density can be derived from equation (8) as in equation (17) while the requirement on heat source power is obtained as equation (18)

$$\dot{q}_{s0R} = \frac{u_{0R} \Delta T_{0R}}{l_{0R}} (\rho_s C_{ps})_R = (\rho_s C_{ps})_R l_{0R}^{-1/2} \Delta T_{0R}^{3/2}, \text{ and} \quad (17)$$

$$P_{0R} = \dot{q}_{s0R} l_{0R} a_{s0R} = a_{0R} l_{0R}^{1/2} \Delta T_{0R}^{3/2}. \quad (18)$$

From equation (16), the relationship between the number of fuel rods and the number of heater rods can be derived by the following equations (19) and (20)

$$a_{s0R} = \frac{a_{0R}}{(\rho_s C_{ps})_R} = N_{rod,R} d_{rod,R}^2, \text{ and} \quad (19)$$

$$N_{rod,R} = \frac{a_{0R}}{\delta_{0R}^2 (\rho_s C_{ps})_R} = k_{sR}^{-1} l_{0R}^{-1/2} \Delta T_{0R}^{1/2} a_{0R}. \quad (20)$$

3.2. Comparison of thermophysical properties of solids

As indicated in Section 3.1, variations in thermophysical properties of solid materials can change heat transfer aspects in the reduced model from the prototype. In particular, to keep the similarity between Ti_{iR} and Q_{iR}, it is therefore necessary to compare the properties, especially between the nuclear fuel rods and the heater rods as these are expected to differ more than the other parts. The URANUS core is loaded with UO_2. In reality, its thermophysical properties are susceptible to be altered by neutron irradiation and temperature distribution [26]. In this study, it is assumed to be fresh fuel and has a low porosity so that its actual density achieves 95% of theoretical density.

As the effective thermophysical properties of a heater rod are strongly dependent on its design, no representative design, which can be utilized for the scaling purpose, might be available. Also, if the actual design is different from what is considered in the design stage, the scaling analysis becomes no longer valid. In this regard, the heater rod used in PILLAR was simultaneously designed iteratively with a supplier so that its effective properties were able to be referenced. The final design of heater rod consists of several layers in the radial direction including sheath, thermal insulation, heating element, and core constituting the radial center as shown in Fig. 1. Among these elements, the use of ceramic materials such as thermal insulation and the radial core greatly influence the effective heat transfer characteristics: the more these materials fill inside a heater rod, the closer to UO_2 its characteristics become. The difference in properties, however, should be considered as it is not negligible.

Stainless steels Type 304 and Type 316L, and nichrome are only taken into account here as potential structural materials. It can be seen from Table 3, which compiles the thermophysical properties of those materials, that the candidates have similar properties to each other, which lead to the structural materials being approximated to be the same. They are also evaluated to have better thermal characteristics compared to those of UO_2 fuel.

3.3. Scaling ratios

According to the design requirements from Section 2.2 and the similarity requirements derived in Section 3.1, the scaling ratios were determined. Most importantly, the length ratios, l_{iR}, for all the components were kept as given in the base design criteria. In addition, the similarity requirements in Ti_{iR} and Bi_{iR} are relaxed since they are physically limited. $\dot{q}_{s0R}$ and $d_{rod,R}$ were designated to be unity to conserve the general behavior of heat source. For a_{0R}, an appropriate value of 1/200 was selected. Additional conditions on physical properties, $(\rho_s C_{ps})_R = 1.200$ and $k_{sR} = 1.129$ by referring to Table 3, were applied. Finally, these decisions also restricted the core power output of PILLAR and the number of heater rods to be installed. Table 4 lists up the scaling ratios adopted for the component design.

4. Facility design and commissioning

4.1. General arrangement of components

As PILLAR was decided to keep the full height and vertical dimensions of URANUS, the final design was given to be a pool configuration with a scale reduction to the radial direction, as shown in Fig. 2 with isometric, cross-sectional, and disassembly views and an actual photograph taken after its assembly at the site. Each LBE region in PILLAR follows the consistent naming convention coherent to URANUS, such as core, upper plenum, riser, heat exchanger, downcomer, and lower plenum, in an order that the primary coolant flows. In view of parts or components, however, this cannot hold, since some regions are physically partitioned by two or three components. The isometric view in Fig. 2(a) depicts that some of the components were necessary to be arranged inside the others by being physically supported.

This condition leads to several practical issues on the manufacturing and commissioning, such as aligning external shells

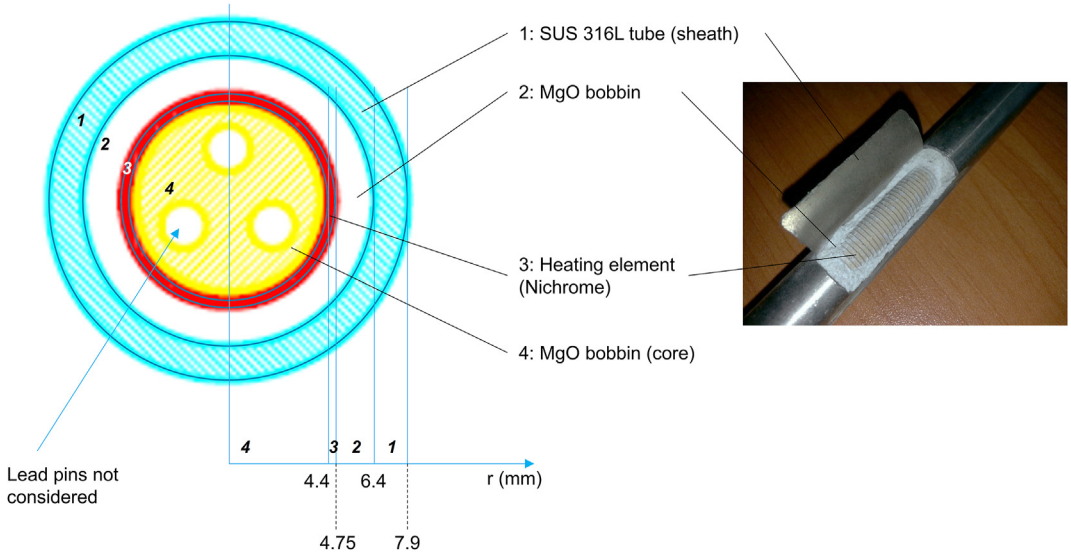

Fig. 1. Cross-sectional design of a PILLAR heater rod (left) and cutaway view of an actual heater rod (right).

Table 3
Comparison of thermophysical properties of nuclear fuel, heater rods, and selected structural materials [24,26].

Material	Property (unit)	Temperature (K)			
		300	400	600	800
SS ANSI 304 [24]	ρ_s* (kg/m^3)	7900	_	_	_
	C_{ps} (J/kg K)	_	515	557	582
	k_s (W/m K)	_	16.6	19.8	22.6
	$\rho_s C_{ps}$ (J/m^3 K)	_	4.07E+06	4.40E+06	4.60E+06
	α_s (m^2/s)	_	4.08E-06	4.50E-06	4.92E-06
SS ANSI 316L [24]	ρ_s* (kg/m^3)	8238	_	_	_
	C_{ps} (J/kg K)	_	504	550	576
	k_s (W/m K)	_	15.2	18.3	21.3
	$\rho_s C_{ps}$ (J/m^3 K)	_	4.15E+06	4.53E+06	4.75E+06
	α_s (m^2/s)	_	3.66E-06	4.04E-06	4.49E-06
Nichrome [24]	ρ_s* (kg/m^3)	8400			
	C_{ps} (J/kg K)	_	480	525	545
	k_s (W/m K)	_	14	16	21
	$\rho_s C_{ps}$ (J/m^3 K)	_	4.03E+06	4.41E+06	4.58E+06
	α_s (m^2/s)	_	3.47E-06	3.63E-06	4.59E-06
Heater rod**	ρ_s* (kg/m^3)	_	_	_	_
	C_{ps} (J/kg K)	_	_	_	_
	k_s (W/m K)	_	_	_	4.70
	$\rho_s C_{ps}$ (J/m^3 K)	_	_	_	3.82E+06
	α_s (m^2/s)	_	_	_	1.23E-06
UO_2 [26]	ρ_s* (kg/m^3)	10413	_	_	_
	C_{ps} (J/kg K)	_	264.3	293.0	305.8
	k_s (W/m K)	_	6.58	5.14	4.17
	$\rho_s C_{ps}$ (J/m^3 K)	_	2.75E+06	3.05E+06	3.18E+06
	α_s (m^2/s)	_	2.39E-06	1.68E-06	1.31E-06

* Density at 300 K is used as a reference in estimation of thermal diffusivity and isothermal heat capacity per unit volume.

** The physical properties of the heater rods are obtained through an iterative design with a supplier. Thermal conductivity, thermal capacity per unit volume, thermal diffusivity coefficient are estimated from a representative design and only the physical properties at 800 K, operating condition, are considered.

and internal components on a concentric axis and preventing them from shaking or moving. In this regard, PILLAR comprises eight components as illustrated in Fig. 2(b) by designing each component in detail to ensure their connectivity and fabricability at the same time.

Under the same philosophy, several design modifications were applied in the detailed design stage. All the components were configured in an ANSI standard profile, SCH 40, to take advantage of supply chain and to exclude dimensional uncertainties from fabrication. This additional distortion is acceptable since the maximum diameter adjusted was about 5 mm. Thus, the hydrodynamic behaviors of the entire system would not be dramatically affected with such a negligible modification. In addition to the dimension adaptation, some parts underwent significant design changes with respect to the prototypic reactor, which will be covered in Sections 4.2 and 4.3. However, no additional components like orifices were added in consideration of inducing extra hydraulic losses in the primary system. As imposed by equation (3) in the scaling design, the prototype and the model should be identical and comparable in terms of the sum of loss coefficients along the flow paths. Owing to the design modifications, the total hydraulic loss of PILLAR was able to be compensated and the ratio is given as $(\Sigma_i (F_i/A_i^2))_R = 0.86$, which is evaluated to be close enough to unity, and thus the slight discrepancy is neglected.

The outermost shell of PILLAR is required to be traced by heaters to heat up the facility before filling the main vessel with LBE; otherwise, the LBE could solidify during its filling. As the tracing heaters would be operated at an elevated temperature higher than 200 °C, a layer of insulation shall be installed for the safety of operators. The insulation also has an important role of minimizing heat loss to the surroundings having a suitable thickness. PILLAR adopted so-called jacket heaters, which are a combination of tracing heaters and insulation. Several jacket heaters are tailored and mounted specifically to the outermost shell considering their vertical arrangements.

4.2. Reactor core simulator

As mentioned in Section 3.2, the heater rod design was made along with the design of facility. The core region of the scaled facility accommodates 27 heater rods, which have an outer diameter of 15.8 mm and the maximum power rating of 15.5 kW, as depicted in Fig. 3(a). Since the geometrical similarities in general layouts and dimensions were conserved, the heater rods were placed in

Table 4
PILLAR design specifications on flow area reduction ratio 1/200.

Specification	Unit	Prototype (URANUS); p	Scale model (PILLAR); m	Scale ratio; m/p
Core power	kW	100000	417	0.00417
Total amount of LBE	ton	470	2.51	0.00534
Core inlet/outlet temperature difference	°C	153	135	0.886
Core inlet (heat exchanger outlet) temperature	°C	304	304	_
Core outlet (heat exchanger inlet) temperature	°C	457	440	_
Total amount of fuel rod/heater rod	_	6480	27	0.00417
Outer diameter of fuel rod/heater rod	m	0.0158	0.0158	1.00
Total heat transfer area	m^2	578.97	2.41	0.00417
Power given by a single fuel rod/heater rod	kW	15.43	15.43	1.00
Linear power given by a single fuel rod/heater rod	kW/m	8.57	8.57	1.00
Heat flux given by a single fuel rod/heater rod	W/m^2	1.73E+05	1.73E+05	1.00
Core volumetric power density	W/m^3	4.37E+07	4.37E+07	1.00
Effective thermal conductivity of fuel rod/heater rod	W/m K	4.17	4.70	1.13
Effective thermal diffusivity of fuel rod/heater rod	m^2/s	1.31E-06	1.23E-06	0.941
Volumetric heat capacity of fuel rod/heater rod	J/m^3 K	3.18E+06	3.82E+06	1.20
LBE average velocity at core outlet	m/s	0.3123	0.2631	0.940
LBE mass flow rate	kg/s	4546.0	21.37	0.00468
Total pressure loss of system	Pa	9743.5	8456.5	0.886

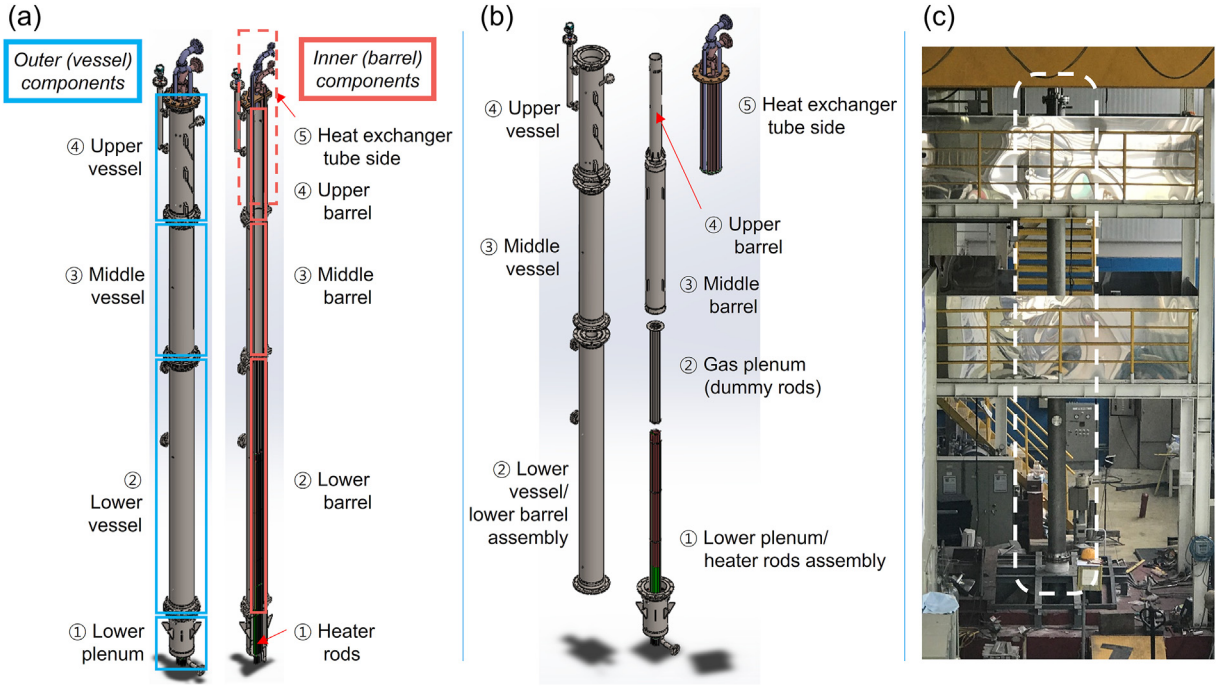

Fig. 2. Final design of PILLAR. (a) Isometric (left) and cross-sectional views (right), (b) exploded view, and (c) photograph in which the facility is highlighted with white dashes.

triangular lattice keeping the pin pitch of 21.3 mm while the strict conservation in height led to the active part, only where the heating element is included, being 1800 mm. Each of the heater rods was determined to be extended from the bottom end of the active part up to 1200 mm to house electrical cables without being exposed to high-temperature, corrosive, liquid metal environments. In this regard, the heater rods were welded on the lower vessel as shown in Fig. 2(b), which also makes the rods free of any unexpected dislocation and a resultant flow channel disturbance. Although this design modification might lead to distortion in flow behavior in the lower plenum, it is thought to be negligible since the LBE in the region would be mostly stagnant.

To suppress the shaking of the rods possibly given by sub-channel flows, three grid spacers are placed together with three skeletal bars along the vertical direction as shown in Fig. 3. They were manufactured out of a 10-mm thick stainless steel plate by electro-discharge machining and wire cutting techniques. The rings on the spacers have a slightly larger inner diameter than the heater rods, leading to them being not physically in contact. In addition, several thermocouples which measure temperature distribution inside the core are on the bottom of the spacers where each of them has three probes.

In the prototypic reactor, the gas plenum region is above the active core, which spans over 1300 mm. As the maximum tube length of a heater rod was limited to 3000 mm, it was determined to simulate the core separately with dummy rods to conserve the flow behavior at the outlet of the core. The dummy rods were designed to have the same outer diameter and geometrical arrangements with the heater rods, being placed above the heater rods.

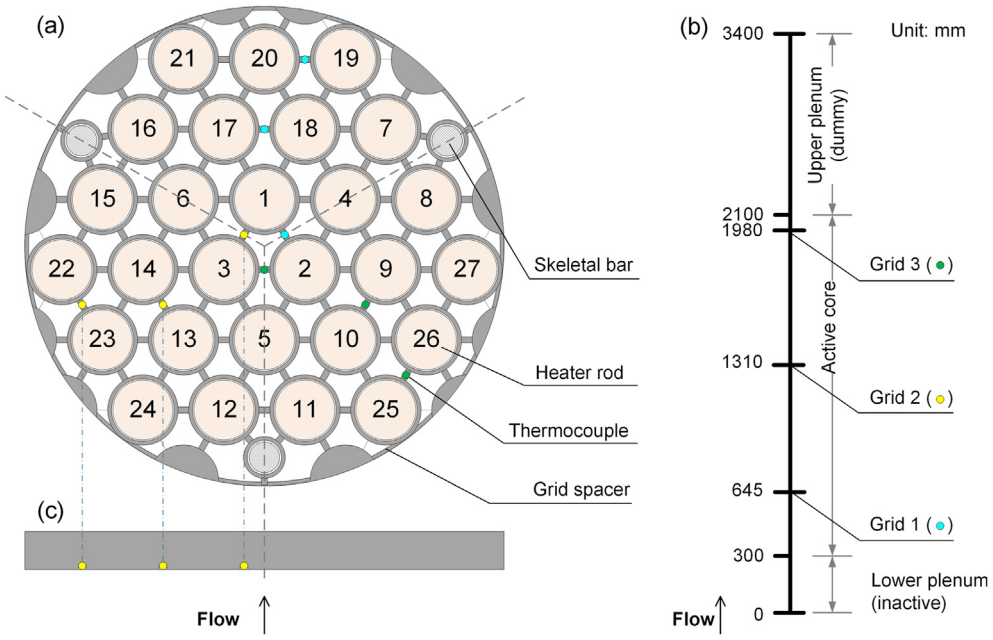

Fig. 3. (a) Layout of core simulator components including heater rods, thermocouples, a grid spacer, and skeletal bars, (b) vertical plan of grid spacers and thermocouples, and (c) side view of a grid spacer and positioning of thermocouple tips. Note that three thermocouples with a same color are mounted on the bottom of each grid spacer. (For interpretation of the references to color in this figure legend, the reader is referred to the Web version of this article.)

As previously stated in Section 4.1, the LBE reflector/shielding region, which surrounds the active core and is filled with stagnant LBE was adapted to a design modification in PILLAR since it was thought to have an almost negligible impact on the flow from a hydrodynamic point of view. However, the geometrical similarity requires this region to be present. Therefore, two internal components, the lower and upper barrels, were re-designed to be concentric, double-walled structures where the enclosed regions are empty. This modification is assessed to be favorable as not only does it contribute to the conservation of radial arrangements but also facilitates prevention of unwanted radial conductive heat transfer from the core to the downcomer region, minimizing heat loss through the internal walls.

4.3. Heat exchanger

The heat exchanger of PILLAR serves as the main heat sink which drives natural circulation flow in non-isothermal conditions, where a major design change was given, as indicated in Section 4.1. In fact, URANUS has eight independent, identical steam generator modules; however, it was difficult to keep the heat transfer areas to-scale with respect to the selected area scaling factor. This fact led to a significant design modification resulting in one single heat exchanger with the key thermal design factors being conserved.

Through this consideration, its final design became a shell-and-tube type heat exchanger, in which the shell side if filled with LBE, while pressurized water flows through the tube side. The shell side is physically partitioned by the riser extended from the active core to the top, and the outer vessel on which the tube side assembly is mounted. The primary LBE can flow through the gap and the sub-channels around the tubes. On the other hand, the tube side assembly consists of several subcomponents: an inlet header which connects to the secondary side, three downcomer pipes in NPS 1¼, schedule 40, as per the ASME standards, a torus water chamber of the same size with the inlet pipes, 21 tubes of 19.05 mm outer diameter where water flows upward, three outlet chambers where seven tubes are merged in each of them, and an outlet header

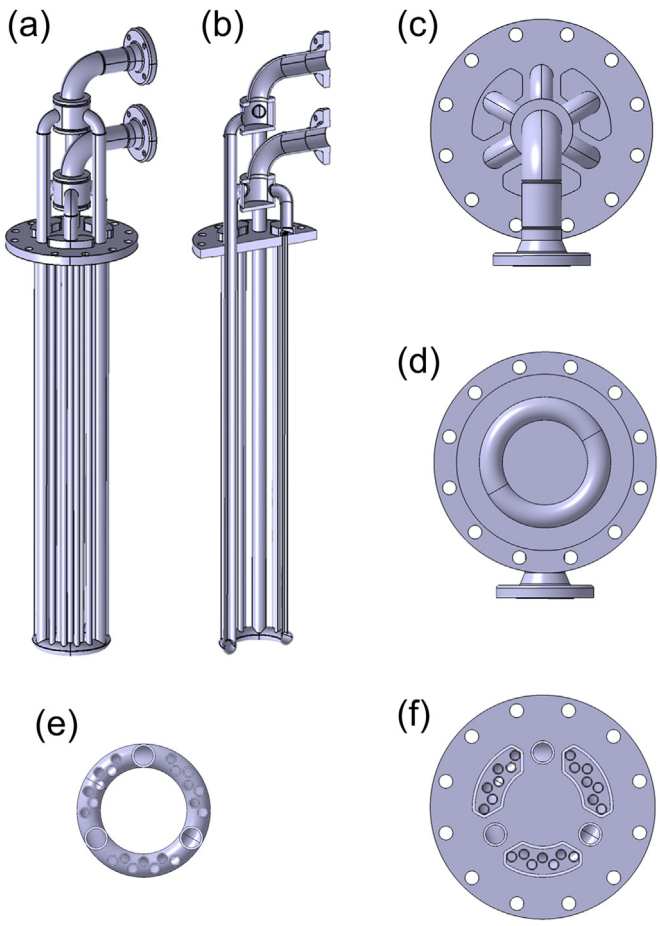

Fig. 4. Three-dimensional model of the PILLAR heat exchanger tube side. (a) Isometric view, (b) cross-sectional view in the vertical direction, (c) top view, (d) bottom view, (e) cross-sectional view of the lower chamber, and (f) cross-sectional view of the upper chambers.

identical to the inlet header, as depicted in Fig. 4. The downcomer pipes and the tubes are arranged in an azimuthal symmetry of 120° to prevent distortion that may occur with local flow distribution. The assembly also forms a pressure boundary by closing the outermost shells of PILLAR.

During operation, a centrifugal pump circulates water, slightly pressurized up to around 6.5 bar, through the closed loop of the secondary side. In this respect, all the constituent parts of tube side assembly were selected to comply with its pressure condition with a suitable margin and the assembly went through a water pressure test at 25 bar to confirm its integrity. A cooling tower serves as an ultimate heat sink in which the water runs through a manifold cooled by air by increasing its heat transfer area significantly.

To give an operational margin on the free surface level, it was decided that the height of the facility was necessarily elongated about 300 mm above the required level, which also affects the active heat transfer length of heat exchanger. In this manner, the length of downcomer pipes and tubes also had to be extended. Additionally, a guide tube was installed on the side of the main vessel from a practical point of view that level control is not viable by inserting a leveling gauge through the narrow gap and subchannels.

4.4. Instrumentation

Table 5 summarizes the instrumentation requirements applied and the role of each instrument, which are in accordance with the objectives and design requirements listed in Table 1. The instrumentation system consists of more than 30 thermocouples, three differential pressure transducers for flow measurement, one waveguide radar level sensor, two gas pressure transducers on the main vessel and LBE storage tank, one electromagnetic flowmeter in the secondary side, and load cells measuring the dead weight of LBE in the storage tank.

Unlike loop-type test facilities, there are additional characteristics to be considered for installation and operation of instruments and sensors in PILLAR due to its shell-in-shell configuration. Namely, it is possible to insert a probe radially through the outermost shell, but technically challenging for the inner regions as they necessitate a complete alignment of all the components, only allowing extremely little tolerance. In addition, too many penetrations by probes are not favorable from the viewpoint of assembly and operation because the probes could interfere with the structure. The instrumentation of inner regions is thus limited.

While reducing the number of probes, the measurement shall be done in important components. This can be compensated by selecting proper positions, taking advantage of symmetrical arrangements, especially in the core region and heat exchanger primary side. Global flow characteristics in such regions can be represented with a limited number of instruments thanks to the periodicity and symmetry in arrangements of heater rods and heat exchanger tubes.

By balancing the two conflicting considerations, the instrumentation plan of the core region was determined. Spatial limitations only allowed thin thermocouples not to take up the free volume of LBE and not to distort the flow. To resolve this, the thermocouple tips of were mounted in the grooves on the bottom of three grid spacers, along the thin bar portions connecting the heater rod support rings, so that they could remain their positions without disturbing the flow, preventing their possible dislocations, as schematically illustrated in Fig. 3(a) and (c). The positions of three thermocouples on a grid spacer were selected to be nearly equidistant along the radial direction, while having an azimuthal symmetry of 120° on each spacer.

The heat exchanger shell side is characterized by several parameters including LBE temperature measured at several vertical positions by relatively thick thermocouples installed through the wall, tube outer wall temperature given by thermocouples mounted on the selected locations, and LBE mass flow rate with a Pitot tube. The flow rate is converted from the local velocity originally measured by a differential pressure transducer. The Pitot tube is also inserted through the outer shell. Similarly to the core region, the probes in the heat exchanger shell side follow the azimuthal symmetry. In this regard, only a 120° segment has the penetrations to relax the alignment requirement otherwise.

4.5. System heat loss evaluation

Prior to starting the actual experiments, a trial run and preliminary tests were conducted to identify the response characteristics of the system. The heat loss evaluation of the system as a whole is of importance in thermal-hydraulic testing, especially on natural circulation in which the behavior of the system depends on the thermal equilibrium between heat source and heat sink. As heat loss to the surroundings is unavoidable, a counter action of compensation is usually taken to ensure the quality of experimental data.

For this purpose, the heating jackets were operated without filling LBE. After the temperature of the whole system was raised, measurements were taken over a few hours. The heating jackets are controlled at a given temperature setpoint by proportional-integral-differential (PID) controllers to regulate electrical outputs in a way that temperature fluctuation is minimized. For the same reason, the secondary side was not filled up during the evaluation as water may contribute to the removal of extra heat from system. A test run was continued for 2–3 h and the test data were averaged over the time span to filter out temporal fluctuations.

Through this procedure, the amount of change on the heater output can be inversely estimated based on the integrated average over measurement span. Hence, utilizing the sum of time average of the electric power given to each of the heating jackets, denoted by subscript i, during the time span from t_0 to $t_0 + \Delta t$, the total amount of heat loss of the system, Q_{loss}, can be defined as in the following equation (21)

Table 5
Requirements of the PILLAR instrumentation system.

System	Type	Parameter to be measured	Precision requirement
Primary system	Type K thermocouple	LBE temperature, environmental temperature, surface temperature	±1 K
	Differential pressure transducer	Local LBE flow velocity, dynamic pressure	±2%
	Absolute pressure transducer	Pressure of cover gas above LBE free surface	0.25% (full range)
	Waveguide radar level sensor	LBE free surface level	±2 mm
Secondary system	Type K thermocouple	Water temperature	±1 K
	Electromagnetic flowmeter	Water volumetric flow rate	0.5% (full range)
	Absolute pressure transducer	Water pressure	0.25% (full range)
Auxiliary system	Type K thermocouple	LBE temperature	±1 K
	Pressure transducer	Pressure of pressure boundary in LBE storage tank	0.25% (full range)
	Load cell	LBE mass in LBE storage tank	±10 kg

$$Q_{loss} \equiv \sum_i \frac{1}{\Delta t} \int_{t_0}^{t_0+\Delta t} Q_i dt. \quad (21)$$

In a strict manner, an adiabatic condition cannot be met due to the (laminar) natural convection by surrounding air. When a particular object lying in the air is at a higher temperature than its surroundings, heat loss occurs primarily through natural convection with a slow rate of heat transfer [27].

$$\frac{\mathrm{Nu}}{\mathrm{Ra}^{1/4}} = const. \quad (22)$$

Both *Nu* and Ra have proportional relationships with *h* and ΔT, the temperature difference between the air and wall surface, respectively. Finally, the heat loss to the environment Q_{loss} can be given as

$$Q_{loss} = c_1 \Delta T^{5/4}, \quad (23)$$

where c_1 is a proportionality coefficient. Once the time average of the power variation and the temperature difference between the surrounding air and the system surface are known, the constant c_1 can be obtained which leads to the integral heat loss with respect to a change in representative temperature of the system.

Considering that the heating jackets will never be removed throughout experimental campaigns, the representative temperature was designated as the surface temperature on the outside of heating jackets, at the middle of the facility in the vertical direction. At the same level, three thermocouples were installed altogether in the radial direction as shown in Fig. 5, one for the surface temperature and the others for the ambient temperatures with a radial offset. The level of the thermocouples was also matched to an internal thermocouple measuring LBE temperature in the downcomer region so that the temperature gradient can also be captured qualitatively.

The temperature variation and time-average interval in the evaluation are shown in Fig. 6 while Fig. 7 presents averaged data points with black squares and a fitted curve in accordance with equation (23) obtained by applying the method of least squares. One average period missing in Fig. 6 is taken from a previous dataset made at the first operation of heating jackets after their installation. The fitted curve is given as $Q_{loss} = 0.09674\Delta T^{5/4}$ where Q_{loss} is in kW and ΔT in °C, respectively, with $R^2 = 0.98815$.

It can be noted that the system heat loss is only about 4 kW even when the temperature difference is 20 °C. Since the actual experimental campaigns were carried out with over 200 kW of core power ratings, it is almost negligible. A confirmation test was arranged by filling the main vessel with LBE and with 250 kW given to the core for longer than 70 h with the secondary side running. Simultaneously, the PID controllers regulated the heating jackets automatically. The obtained results are shown in Fig. 8, where only 70-h data after natural circulation was established are given. At the beginning, a relatively large amount of electrical power was supplied, which was followed by a gradual, discrete reduction in power, and eventually most of the PID controllers were turned off. The system temperature fluctuation seems to be rather dominated by the ambient air temperature, not by the tracing heaters. In terms of thermal balance between the primary and secondary sides, the heat compensation by the heating jackets has only a limited impact. Therefore, it was confirmed that the heating jackets do not have a remarkable influence on the system in high core-power conditions, since the main vessel is sufficiently insulated.

The experience indicates that even though a power of 250 kW or more was applied to the core, the temperature difference between the outermost surface and ambient air was around 20 °C. It is due to the fact that the entire system has a small surface area relatively to its volume and the main heat source enclosed by the external region, such as the downcomer, leading to an effective heat insulation. Therefore, it was concluded that the heat loss of the entire system is so negligible that it will not affect the experimental results very much. In the experimental conditions, the heating jacket

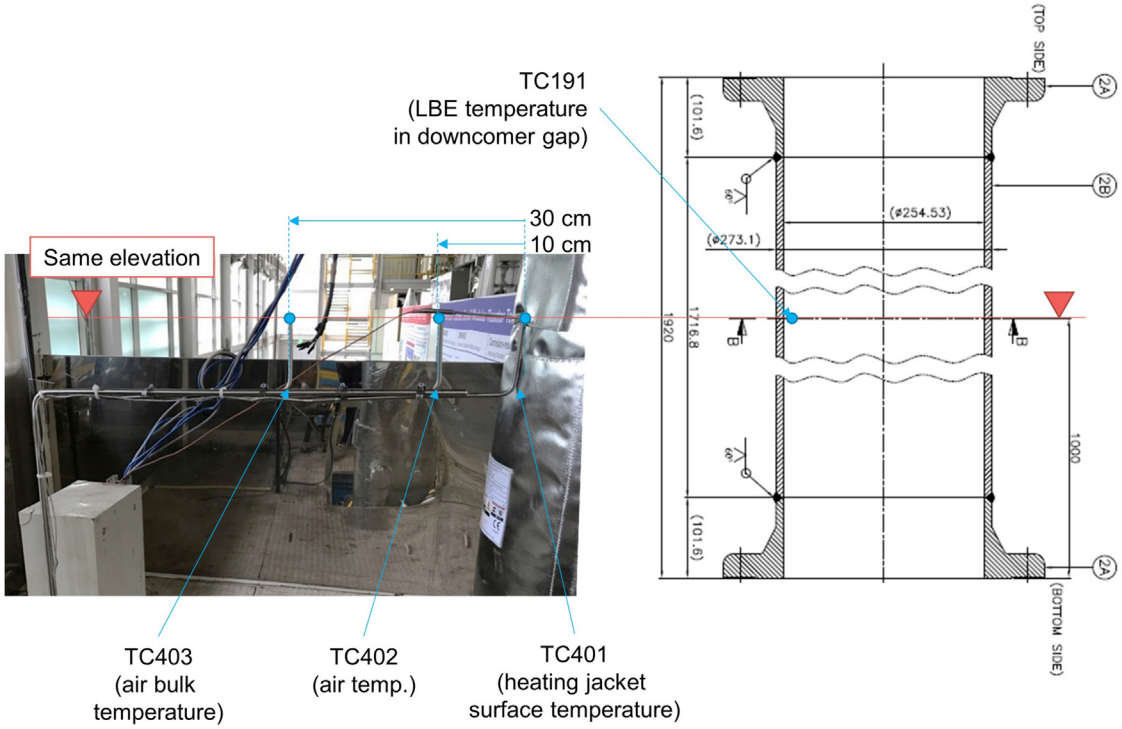

Fig. 5. Locations of thermocouples for system integral heat loss evaluation.

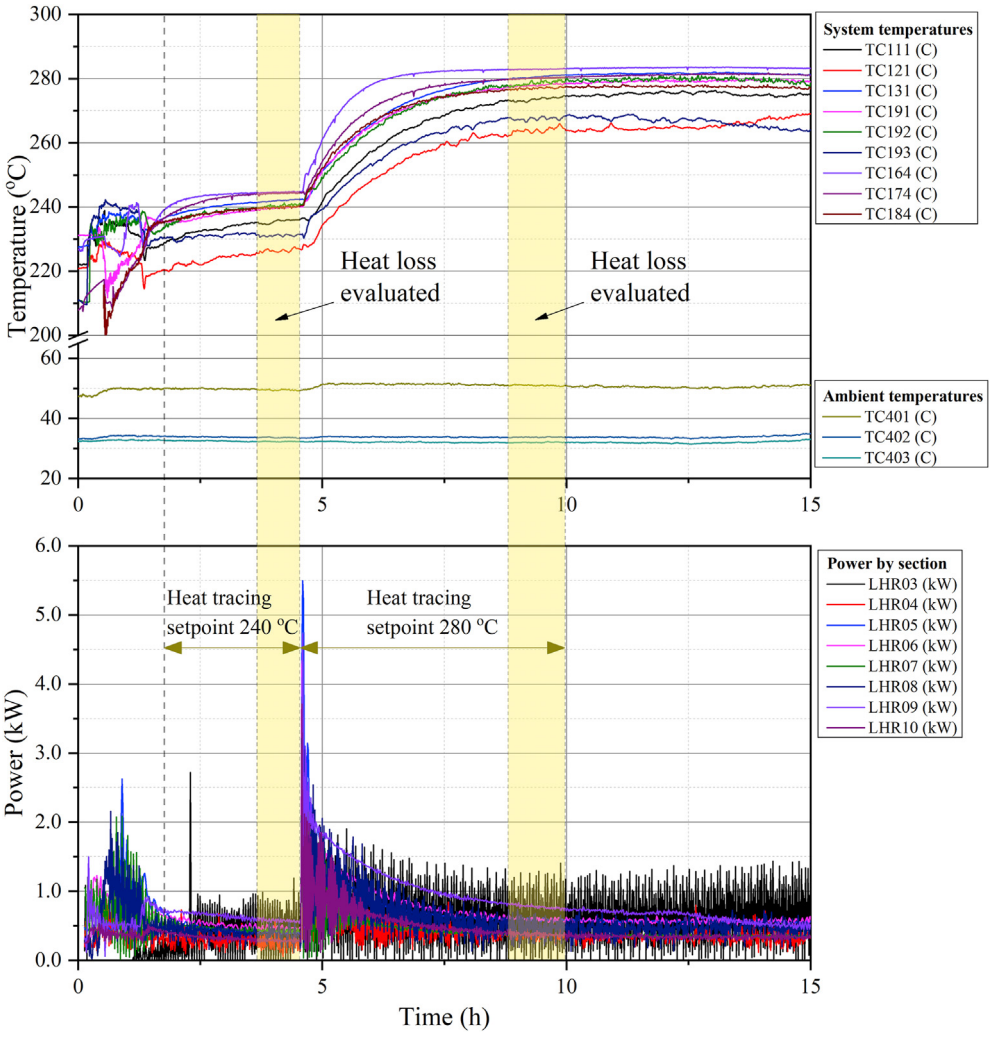

Fig. 6. System integral heat loss evaluation test results.

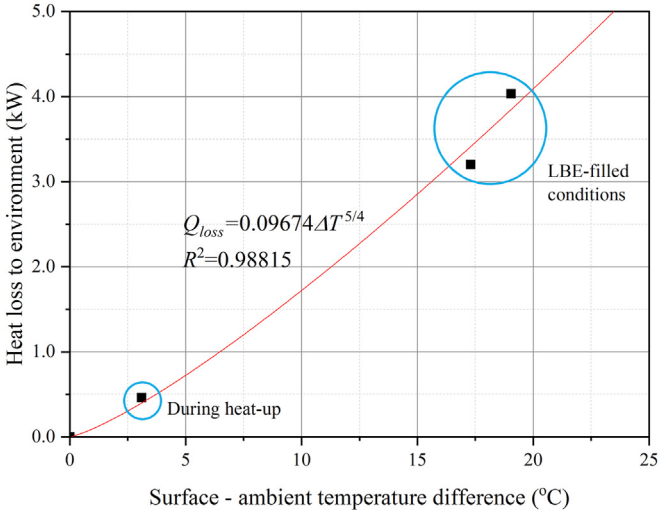

Fig. 7. PILLAR primary system heat loss as function of temperature difference between the surface and ambient temperatures.

controller is set at a slightly lower temperature than the coolant temperature so that only a small amount of heat loss is compensated from time to time.

5. Experimental

5.1. Procedures

Prior to running a new test, several preparation steps have to be undergone. First of all, LBE in the storage tank needs to be melted and all the parts in the primary system are heated higher than 200 °C. The main vessel is filled up with LBE by pressurizing the storage tank with argon gas. By trial and error, the target free surface level is fine-tuned as it decides the active heat transfer length of the heat exchanger so that it must be in an acceptable range. To prevent the unwanted solidification of LBE during filling, the heat exchanger tube side is left empty. Once filling is done, a motor-operated valve on the LBE drain line is closed to isolate the primary system. In addition, the storage tank pressure needs to be released so that the LBE in the main vessel can be drained by gravity in an emergency condition. The secondary side is filled up with water allowing boiling in the heat exchanger by opening a pressure relief valve on the top until no steam comes out of the valve. When the water loop becomes full of water, pressurization is done passively owing to a bladder-type accumulator.

Once the system is ready, a new run is initiated by increasing the electrical power supplied to the heater rods in the core region. To help the natural circulation develop faster, the secondary side can

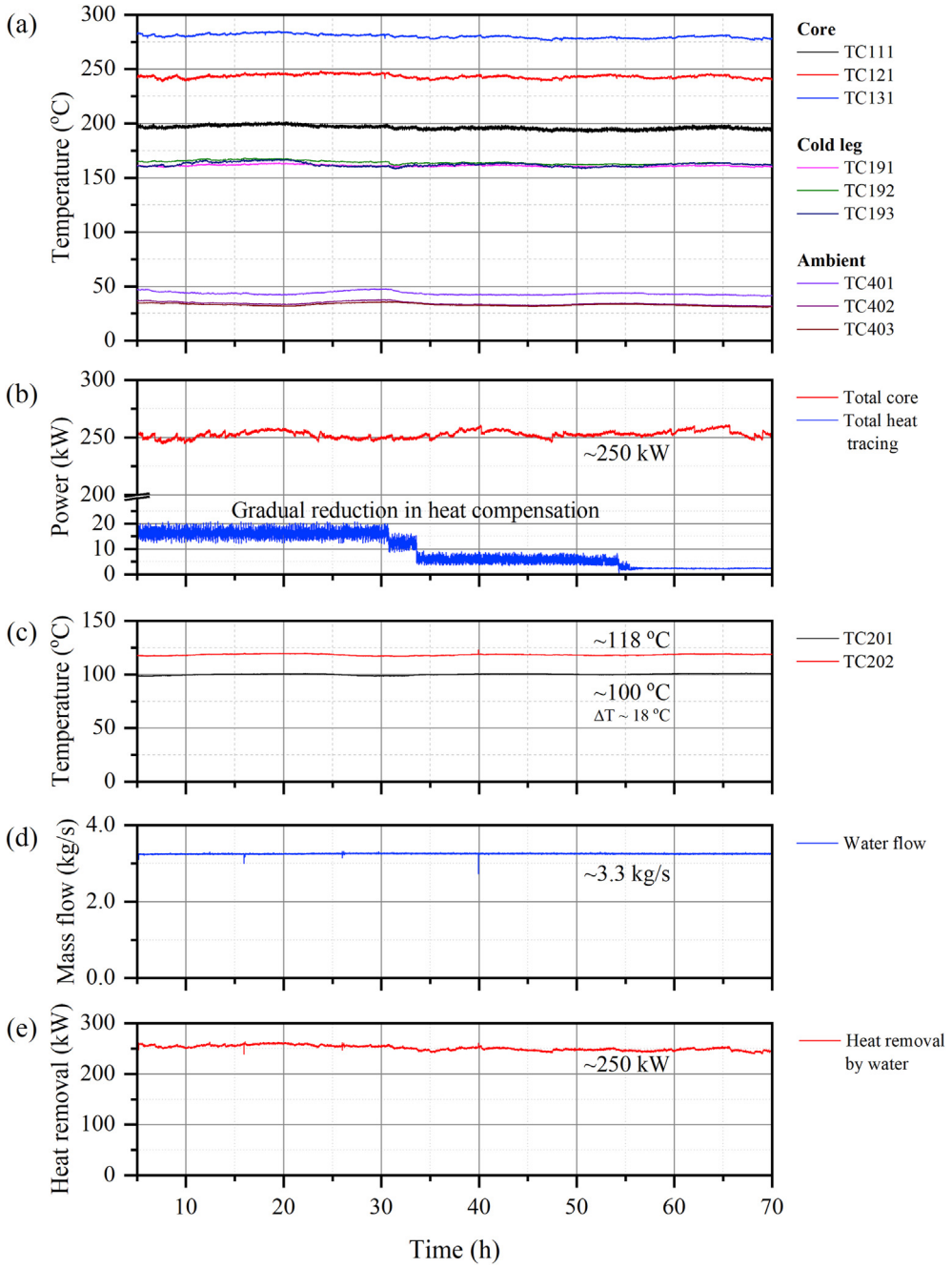

Fig. 8. PILLAR system response to the variation in heat tracing. (a) Primary side temperatures, (b) core power and heat compensation by tracing heaters, (c) secondary side temperatures, (d) water mass flow, and (e) estimated heat removal rate by water.

also be operated. As discussed in Section 4.5, all the heating jackets are supposed to be turned off during a test run, as long as the core power is high enough, since heat loss would be negligible.

Any change or manipulation of experimental conditions leads to the system reacting to that, to reach a new state. At the beginning, the system response is rapid, but it gradually slows down: remarkable transients occur within the first 10 min, and the temperature and flow fields are stabilized slowly afterwards. Mostly, it almost gets to a steady state condition after 1 h from the beginning of a test. For steady-state experiments, the system is left undisturbed for a few hours to collect the data to be averaged over time to maximize the quality by reducing statistical random errors.

A transient test run is then started from a steady state by changing any parameters of interest. It should be done from a steady state which is monitored over at least 2 h since the initial condition affects the system behavior as well. Once the system is perturbed, the same approach to leave the system for 2 h is applied.

Thanks to the simple design of the main vessel, no oxygen control system was thought to be necessary since the oxygen inleak rate might be very little. However, to minimize free surface oxidation, which may be important when drained, the cover gas region on the top of the main vessel was purged with 4%-H_2 (Ar balance) gas with a negligible flow rate during the tests all the time. At the same time, the storage tank was also maintained as an inert atmosphere with Ar, to prevent the remaining LBE from oxidation.

5.2. Steady-state natural circulation tests

Table 6 sums up the steady-state experimental results conducted in PILLAR. Due to the passive nature of natural circulation, only few independent variables are available, which involve the electrical power to the core, the secondary side flow rate and inlet temperature. As stable and precise boundary conditions contribute to the validity of code benchmark, which will be delineated in Section 6, the secondary side conditions including the inlet temperature, water mass flow rate, and pressure were kept nearly constant while the heat source conditions in terms of the core power ratings are varied. In this study, the post-processed data from seven test runs at 249, 253, 284, 293, 302, 306, and 315 kW are presented with by averaging the recorded over at least 2 h as suggested in Section 5.1.

In all the cases, the discrepancies in heat balance between primary and secondary sides were estimated less than 5%. Considering no heat compensation was applied, it is also able to be indirectly confirmed that PILLAR is equipped well with a sufficient thickness of insulation so that it can effectively manage heat loss to the environment. Nevertheless, inevitable daily temperature fluctuations were observed.

5.3. Transient natural circulation tests

Unlike the steady-state experiments in which the final states are determined distinctively, transient test needs to be defined by initial and final states. Among several experimental sets conducted, only four cases are presented in this article as listed in Table 7 to avoid redundancy since each type of tests showed a similar and consistent response. The test runs are carried out, which were driven by two types of perturbation with respect to core power and water flow rate of the secondary side.

The core power transient cases include T-01 and T-02, which relates to the power increase and decrease from certain steady states. The test results are shown in Fig. 9 and Fig. 10, which respectively represent cases T-01 and T-02. It is noted that the experimental results are plotted together with the transient simulation results, which will be covered in Section 6.3. Both cases were initiated by instantaneous power level changes as much as 30 kW within 1 s while keeping all the other parameters constant. The system almost reached a new steady state in each case and the primary side flow rates were stabilized and saturated within 15 min. At the beginning of perturbation, it can be also observed that the primary mass flow shows a slight overshoot and undershoot in each case. Compared to this, the core inlet and outlet temperatures rose or decreased, and finally reached the new states mildly. As the water inlet temperatures were fixed, the outlet temperatures responded to balance the energy transport from the primary side to the secondary side. As the average temperatures of the water side vary, those of LBE also followed the transients.

On the other hand, the secondary water flow transients were conducted under cases T-03 and T-04, which are illustrated in Fig. 11 and Fig. 12, respectively. The flow rate varied for 0.5 kg/s over 1 min linearly whereas all the other boundary conditions were kept constant similarly to cases T-01 and T-02. A temporary overcooling or undercooling was drawn by the gradual changes in water flow, while a negligible effect was observed in the core inlet temperature. As the rate of change in the secondary water flow is far lower in cases T-03 and T-04, the system could follow slow transients with which the system did not undergo an undershoot or overshoot.

The experimental results shown in this section can be extended to the transient behaviors of not only URANUS but also passive SMRs. As PILLAR simulates nuclear fuel with electrical heaters, no reactivity feedback can be exactly represented. Furthermore, the fast neutron generation time in a fast neutron spectrum makes the full simulation impossible. Nevertheless, a rapid power incursion or drop is still comparable as long as the heater rods react to the power input change instantly. Hence, some cases of instant or step power transient could be realistic. Moreover, the overcooling and/or undercooling given by the secondary side flow rate change will affect the primary side, in terms of reactivity insertion in a real reactor. Meanwhile, similar to the test results, the secondary side of the actual reactor would require more time to be saturated with regard to the time needed for the primary side.

6. System code simulation

6.1. MARS-LBE code and system nodalization

The simulation of PILLAR experimental results was conducted with a one-dimensional system thermal-hydraulics code MARS-LBE, which originated from MARS 3.1 release [28], dedicated to applications on heavy liquid metal reactor systems. It features property tables updated for LBE according to the LBE handbook [5]. In addition, some internal routines were modified, which facilitates a more accurate simulation as the code treats heat transfer from a liquid domain to an adjacent solid region or vice versa with a dedicated subroutine which selects a proper convective heat transfer correlation according to the flow conditions in the domain while its original version did not contain suitable correlations for liquid metals. In this regard, the Seban-Shimazaki correlation [25], equation (14), was included to cover a wide range of application to LBE flows. The latest release, MARS-LBE 3.11, was already benchmarked and validated with LBE loop data [29,30].

The hydrodynamic systems of PILLAR were nodalized into several one-dimensional components with about 210 computational cells as shown in Fig. 13. Most of the parts were able to be

Table 6
Selected steady-state natural circulation test results and boundary conditions.[a]

ID	Primary (LBE) side					Secondary (water) side			
	Core power (kW)	Cold leg temperature (°C)	Hot leg temperature (°C)	Temperature difference (°C)	Mass flow rate (kg/s)	Inlet temperature (°C)	Outlet temperature (°C)	Mass flow rate (kg/s)	Pressure (bar)
S-01	249	163.46	252.53	89.07	18.55	102.5	119.8	3.30	6.20
S-02	253	161.54	251.17	89.63	18.67	100.1	118.2	3.26	6.39
S-03	284	170.74	268.56	97.83	19.25	102.2	122.0	3.31	6.17
S-04	293	172.48	272.74	100.3	19.49	102.3	122.7	3.32	6.07
S-05	302	173.89	276.50	102.6	19.63	102.6	123.6	3.31	6.13
S-06	306	170.60	274.44	103.8	19.70	101.2	122.7	3.23	6.33
S-07	315	176.30	282.82	106.5	19.85	102.5	124.4	3.32	6.08

[a] All the values are mean values based on measured data over at least 2 h.

Table 7
Selected transient natural circulation tests and boundary conditions.

ID	Parameter varied	Main parameters				Boundary conditions	
		Core power (kW)	Water flow rate (kg/s)	Period of change (s)	Rate of change (kW/s or kg/s/min)	Water inlet temperature (°C)	Water pressure (bar)
T-01	Core power	210 → 240	3.5	1	+30	103.0	6.43
T-02	Core power	240 → 210	3.5	1	−30	103.2	6.40
T-03	Water flow rate	240	3.5 → 4.0	60	+0.5	103.1	6.52
T-04	Water flow rate	240	4.0 → 3.5	60	−0.5	102.5	6.47

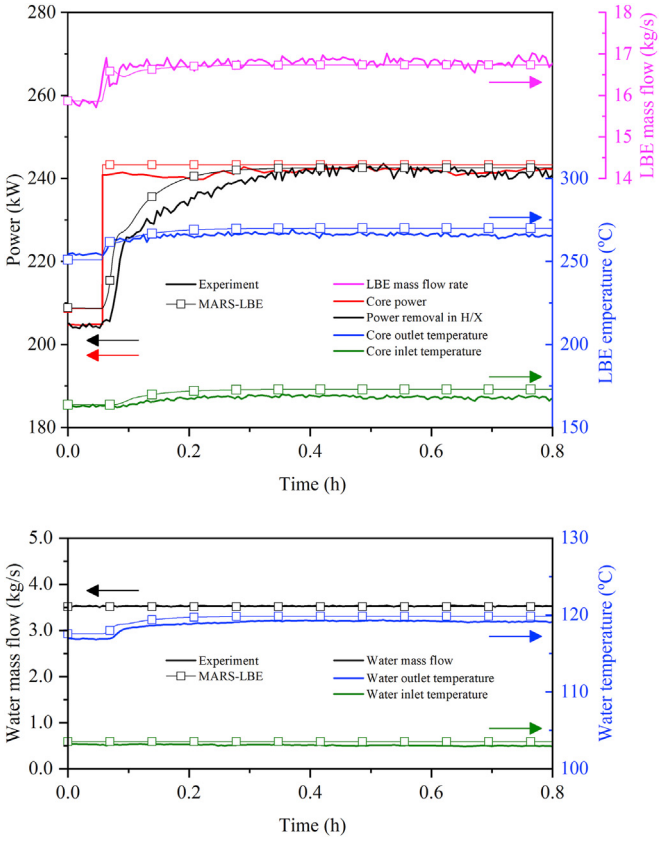

Fig. 9. Experimental and MARS-LBE simulation results on step power increase (case T-01).

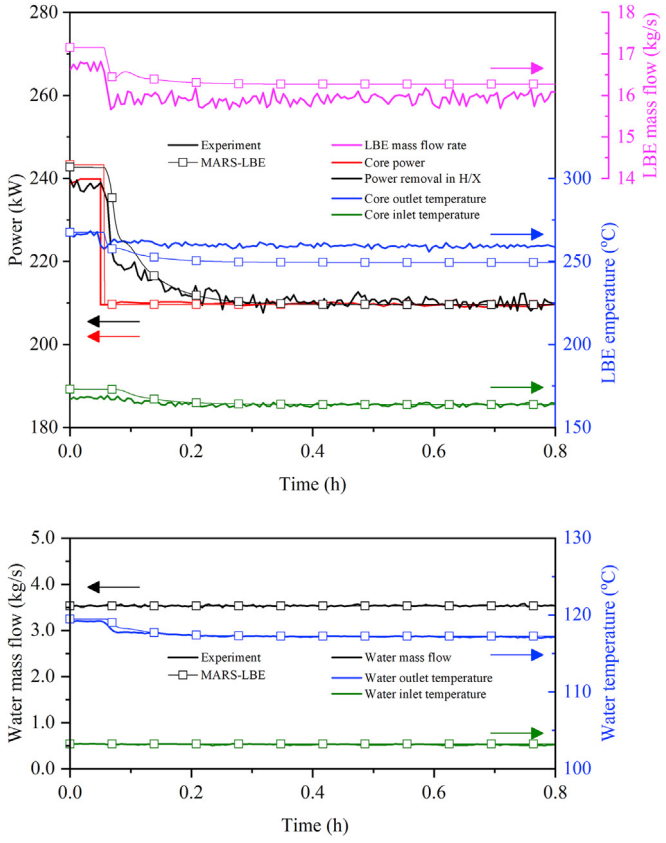

Fig. 10. Experimental and MARS-LBE simulation results on step power decrease (case T-02).

arranged with pipes or annuli, and junctions connecting each other, while the use of pipes forces to simulate the flow inside the core and upper plenum being averaged over whole flow areas. In fact, the mass, momentum, and energy conservation equations in MARS are formulated in the two-fluid model which utilizes the volume- and time-averaged parameters of vapor and liquid phases for such one-dimensional components [28]. However, as LBE practically does not boil under temperatures of interest, the formulations fall into the equivalent single-phase equations without phase change and thus without exchange of parameters across the phases interface.

In addition to the system nodalization, the boundary conditions are given by the core power rating through the heat structure for heater rods, and the secondary feedwater conditions including mass flow rate, inlet temperature, and pressure. Assuming the system is adiabatic, no heat loss to the environment was modeled. For the convective heat transfer coefficient on water side, the Dittus-Boelter relation [31], $Nu = 0.023\ \mathrm{Re}^{0.8}\ \mathrm{Pr}^{0.4}$, was utilized.

Several solid regions in the heater rods, heat exchanger tubes, and the inner shells between the downcomer and riser or core regions were included as heat structures, to take into account the effect of thermal inertia. An equivalent model was used by interpreting a rod having concentric radii with uniform and homogeneous properties, neglecting the lead pin arrangement inside the MgO bobbin. The radius of each region can also be found in Fig. 1 and the thermophysical properties are taken from Table 3.

6.2. Code benchmark on steady-state natural circulation tests

This section describes the code benchmark results with MARS-LBE on the steady-state natural circulation tests given in Section 5.2. As boundary conditions, the core power rating and secondary side conditions including water inlet temperature, mass flow rate, and pressure were designated to the time-dependent volumes and junctions, and heat structures equivalent to the test runs listed in Table 6.

The code was made to run to find a steady-state solution for each case. The benchmark results are compared with the simulation results as shown in Fig. 14. Among a number of parameters

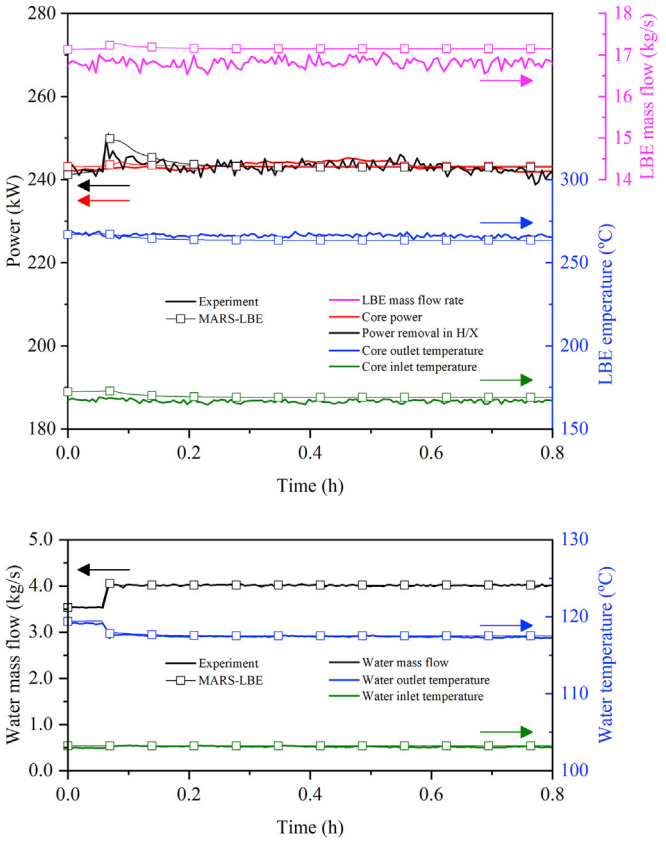

Fig. 11. Experimental and MARS-LBE simulation results on a ramp-up of secondary water flow (case T-03).

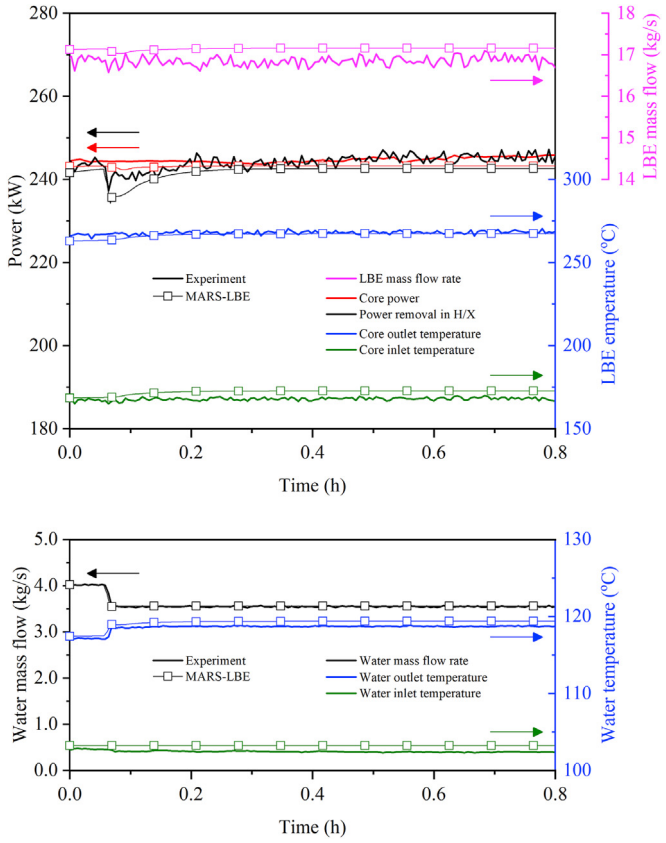

Fig. 12. Experimental and MARS-LBE simulation results on a gradual decrease in the secondary water flow (case T-04).

estimated, two major parameters, including the primary side mass flow rate and the temperature difference over the core inlet and outlet, are taken into account as these parameters are able to represent the system conditions under natural circulation and thus the validity of the code. As can be seen in Fig. 14(a) and (b), the deviations between the experimental and simulation results lie within ±3% bands, both in LBE mass flow rate and temperature difference. Through this benchmark, it is confirmed that MARS-LBE is capable of capturing integral system behaviors, which can be extended to the thermal-hydraulic design and safety analysis of passive small modular reactors employing LBE as primary coolant. However, some specific designs where local flow effects should be considered, this benchmark does not hold as the code itself is not able to model them properly.

6.3. Simulation of transient natural circulation experiments

The benchmark exercise in the previous section, however, does not ensure whether MARS-LBE also has an acceptable capability of transient simulation. As a qualitative approach, the transient simulation results are compared to the experimental runs as described in Section 5.3.

In MARS-LBE, any parameter can be altered at a specific simulation time or over a period with constant or varying rates of change using time-dependent components and control system components [28]. In general, the former directly deals with specific parameters in a hydrodynamic system, by directly adapting boundary conditions such as temperature, pressure, mass flow rate, and heat flux. The latter is a logical relation triggered by one or more conditions of the system, which can be defined by the Boolean operations. In this study, only several time-dependent components were used as the experimental conditions of the transient tests and how the system was maneuvered were almost similar to the way that the time-dependent components work. In this regard, a transient run was initiated by feeding a pre-calculated steady state result to the code as an initial condition.

The four figures already illustrated in Section 5.3, Figs. 9–12, show the simulation results together with the monitored records during transient test cases T-01 to T-04, respectively. Qualitatively speaking, the simulation agrees well with the measured, in all the cases. Some specific behaviors which can be observed in the experiments, such as the time delay for tube side heat transfer saturation, the water outlet temperature variation due to enthalpy change, and the instantaneous tube side heat transfer jump or drop from flow rate changes, are also able to be captured by MARS-LBE, which suggests that the code can also offer a high-fidelity simulation of transient natural circulation cases.

7. Summary and conclusions

The cost competitiveness and versatility are thought to be the major incentives of SMRs over large-scale reactors. Motivated by various promising attributes of lead and LBE, a number of SMRs which adopt those heavy liquid metals as primary coolants are proposed and under development along with the growing worldwide interest in such reduced-scale reactor systems. Despite the fact that experimental demonstration is crucial not only to the system and component designs but also to the licensing, the necessity of test facilities dedicated to liquid metal cooled SMR systems has been overlooked. PILLAR is in this respect commissioned

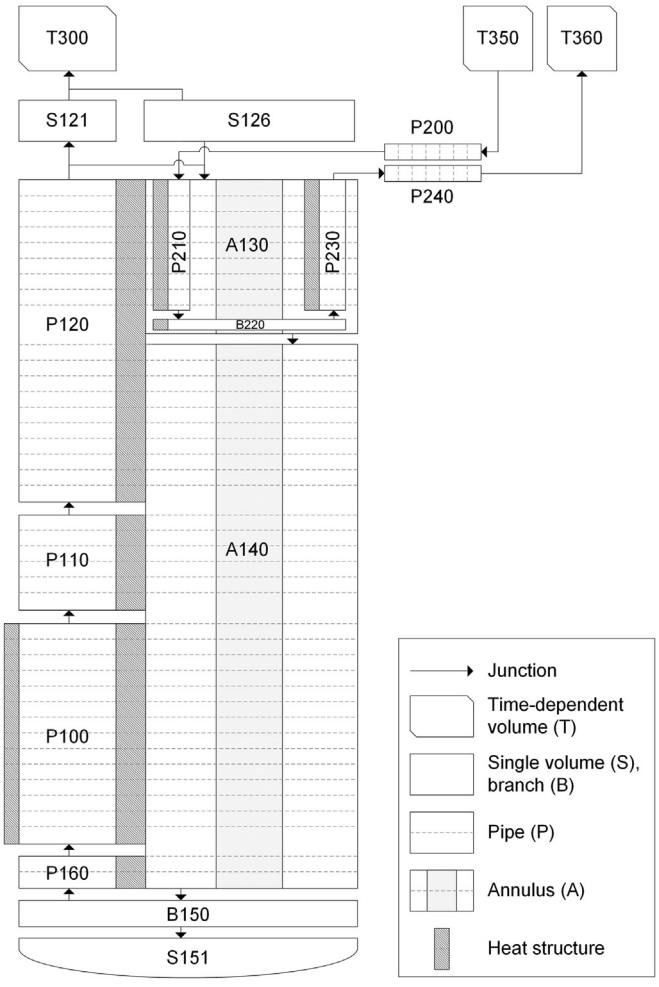

Fig. 13. Nodalization map of the PILLAR primary and secondary sides.

to serve as a test bed which facilitates experimental activities on the integral system behaviors that a passive LBE-cooled system often faces. Furthermore, the test results obtained from the facility can be utilized for the research and development of SMRs.

The scale design of PILLAR was made through a scaling analysis by keeping the height ratio to be unity from its prototypical reactor design of URANUS whereas the flow area was reduced uniformly in the radial direction, about 1/200. The constituent components were designed properly to represent the hydraulic behaviors to be similar while some of them underwent slight adaptations to fit the industrial standards, within acceptable and negligible ranges. The reactor core is simulated by several electrical heaters which feature a similar radial arrangement given in a triangular lattice while reducing the number of rods proportional to the flow area reduction. A single-module, shell-and-tube type heat exchanger represents the eight modules of steam generators in the prototype. Data acquisition is done by more than 30 channels of instruments which record temperatures, local velocities, absolute and gauge pressures, weight, current draw and voltage. Thanks to the insulation as thick as 5 cm enclosing the outermost shells, heat loss could be minimized and well-managed with tracing heaters, which allow us to run a test without compensating for the energy mismatch between the primary side and secondary side, which may lead to an ill-conditioned result otherwise.

With PILLAR, several natural circulation test runs were conducted, only selected results are reported in this paper. The steady-state results were summarized by obtaining mean values of the reported data in time over at least 2 h once the system reached a new state and no significant change was observed. The runs were made at seven different core powers while the secondary side conditions were kept the same as much as possible. In addition, a few transient runs were carried out, which were initiated from a steady state by giving a perturbation in terms of the core power rating or secondary side flow rate and temperature. Among others, four transient runs were reported, which include the instantaneous power incursion and drop, and the gradual increase and decrease in water flow rate over 1 min. These transients are able to represent various safety cases and operating conditions such as load-following mode.

The steady-state test results were utilized for the benchmark of a system code, MARS-LBE. The benchmark results show that the code was able to provide high-fidelity simulation results, within ±3% offsets. Through this activity, it was able to confirm that its simulation capability was extended to the design and safety analysis of heady liquid metal integral pool systems beyond the loop configurations with which the code had been experimentally validated. The qualitative comparisons on the transient test results

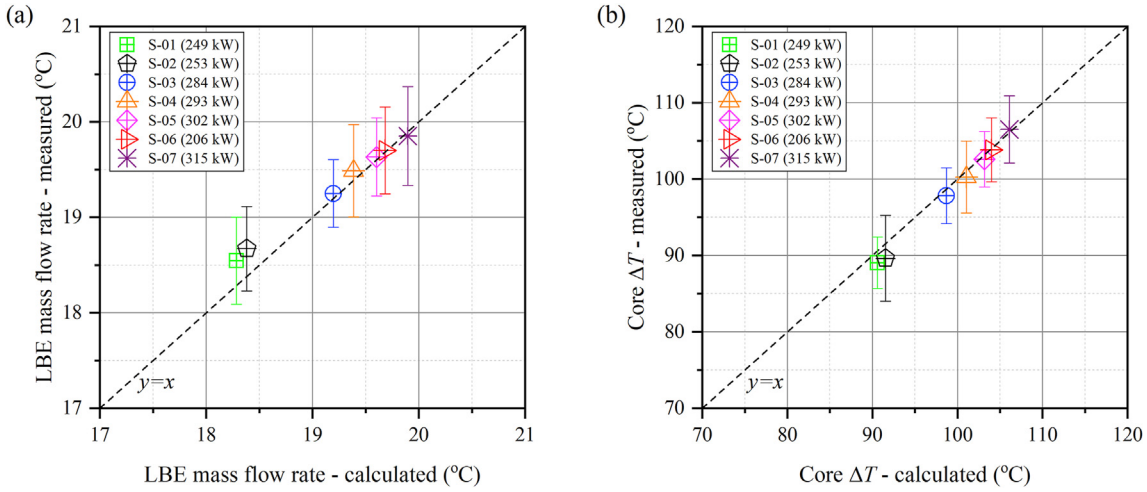

Fig. 14. MARS-LBE benchmark results compared to PILLAR steady-state natural circulation test results. Comparison on the measured versus simulated (a) LBE mass flow rates and (b) core inlet − outlet temperature difference.

were also conducted, which show that the code is capable of capturing the integral system behaviors.

Declaration of competing interest

The authors declare that they have no known competing financial interests or personal relationships that could have appeared to influence the work reported in this paper.

Acknowledgments

This work was supported by a National Research Foundation of Korea (NRF) grant funded by the Ministry of Science and ICT, Republic of Korea (NRF-2021M2D1A1019061). The authors would like to express their gratitude to Mr. Y.M. Park and his colleagues at Moojin Keeyeon for their design support and fabrication of PILLAR, and also to Mr. B.S. Kim and his coworkers at Samjin for their technical support.

References

[1] IAEA, Advances in Small Modular Reactor Technology Developments, International Atomic Energy Agency, Vienna, Austria, 2020.
[2] D.T. Ingersoll, M.D. Carelli, Handbook of Small Modular Nuclear Reactors, second ed., Woodhead Publishing, Duxford, United Kingdom, 2020.
[3] M.R. Islam, H.A. Gabbar, Study of small modular reactors in modern microgrids, International Transactions on Electrical Energy Systems 25 (9) (2015) 1943–1951.
[4] A. Lokhov, V. Sozoniuk, G. Rothwell, M. Cometto, H. Paillere, M. Crozat, T.J. Kim, M. McGough, D. Ingersoll, R. Rickman, Small Modular Reactors: Nuclear Energy Market Potential for Near-Term Deployment, Organisation for Economic Co-Operation and Development, Paris, France, 2016.
[5] OECD Nuclear Energy Agency, in: C. Fazio, et al. (Eds.), Handbook on Lead-bismuth Eutectic Alloy and Lead Properties, Materials Compatibility, Thermal-hydraulics and Technologies, OECD Nuclear Energy Agency, Paris, France, 2015, 2015.
[6] K. Tuček, J. Carlsson, H. Wider, Comparison of sodium and lead-cooled fast reactors regarding reactor physics aspects, severe safety and economical issues, Nucl. Eng. Des. 236 (14) (2006) 1589–1598.
[7] L. Cinotti, P. Briger, G. Giacomo, Simplification, the atout of LFR-AS-200, in: International Conference on Fast Reactors and Related Fuel Cycles: Next Generation Nuclear Systems for Sustainable Development (FR17), 2017. Yekaterinburg, Russia.
[8] J. Wallenius, S. Qvist, S. Bortot, I. Mickus, J. Ejenstam, P. Szakalos, SEALER: a small lead-cooled reactor for power production in the Canadian Arctic, in: International Conference on Fast Reactors and Related Fuel Cycles: Next Generation Nuclear Systems for Sustainable Development (FR17), 2017. Yekaterinburg, Russia.
[9] J. Zhang, R.J. Kapernick, P.R. McClure, T.J. Trapp, Lead–bismuth eutectic technology for Hyperion reactor, J. Nucl. Mater. 441 (1–3) (2013) 644–649.
[10] A.V. Zrodnikov, G.I. Toshinsky, O.G. Komlev, Y.G. Dragunov, V.S. Stepanov, N.N. Klimov, I.I. Kopytov, V.N. Krushelnitsky, Nuclear power development in market conditions with use of multi-purpose modular fast reactors SVBR-75/100, Nucl. Eng. Des. 236 (14–16) (2006) 1490–1502.
[11] S. Choi, J.-H. Cho, M.-H. Bae, J. Lim, D. Puspitarini, J.H. Jeun, H.-G. Joo, I.S. Hwang, PASCAR: long burning small modular reactor based on natural circulation, Nucl. Eng. Des. 241 (5) (2011) 1486–1499.
[12] Y.-H. Shin, S. Choi, J. Cho, J.H. Kim, I.S. Hwang, Advanced passive design of small modular reactor cooled by heavy liquid metal natural circulation, Prog. Nucl. Energy 83 (2015) 433–442.
[13] T.J. Morton, Primary System Test Facility Review, Idaho National Laboratory, Idaho Falls, ID, United States, 2019.
[14] H.-S. Park, B.-Y. Min, Y.-G. Jung, Y.-C. Shin, Y.-J. Ko, S.-J. Yi, Design of the VISTA-ITL test facility for an integral type reactor of SMART and a post-test simulation of a SBLOCA test, Science and Technology of Nuclear Installations 2014 (2014) 840109.
[15] S. Grewal, E. Gluekler, Water simulation of sodium reactors, Chem. Eng. Commun. 17 (1–6) (1982) 343–360.
[16] D. Weinberg, D. Suckow, U. MUller, H. Hoffmann, The Transferability to Reactor Conditions of Thermohydraulics Model Investigations of Decay Heat Removal. Roc. Int. Fast Reactor Safety Mtg., 1990. Snowbird, Utah.
[17] Y. Eguchi, H. Takeda, T. Koga, N. Tanaka, K. Yamamoto, Quantitative prediction of natural circulation in an LMFR with a similarity law and a water test, Nucl. Eng. Des. 178 (3) (1997) 295–307.
[18] H. Takeda, T. Koga, O. Watanabe, Experimental and computational simulation for natural circulation in an LMFBR, Nucl. Eng. Des. 140 (3) (1993) 331–340.
[19] K. Van Tichelen, F. Mirelli, M. Greco, G. Viviani, E-SCAPE: a scale facility for liquid-metal, pool-type reactor thermal hydraulic investigations, Nucl. Eng. Des. 290 (2015) 65–77.
[20] X.-N. Chen, On LBE natural convection and its water experimental simulation, Prog. Nucl. Energy 78 (Supplement C) (2015) 372–379.
[21] M. Ishii, I. Kataoka, Scaling laws for thermal-hydraulic system under single phase and two-phase natural circulation, Nucl. Eng. Des. 81 (3) (1984) 411–425.
[22] M. Ishii, S.T. Revankar, T. Leonardi, R. Dowlati, M.L. Bertodano, I. Babelli, W. Wang, H. Pokharna, V.H. Ransom, R. Viskanta, et al., The three-level scaling approach with application to the purdue university multi-dimensional integral test assembly (PUMA), Nucl. Eng. Des. 186 (1) (1998) 177–211.
[23] S.H. Jeong, Development of an Integral Test Loop, HELIOS and Investigation of Natural Circulation Ability for PEACER, Ph.D. Thesis, Seoul National University, Seoul, Korea, 2006.
[24] S.J. Hong, D.Y. Lee, Scaling and Design of Integral Test Facility Simulating 600MWe SFR (Korean Version), FNC Technology Co., and Korea Atomic Energy Research Institute, 2012.
[25] R.A. Seban, T. Shimazaki, Heat Transfer to a Fluid Flowing Turbulently in a Smooth Pipe with Walls at Constant Temperature, California Univ., Berkeley (USA), 1949 (Inst. of Engineering Research).
[26] S. Popov, J. Carbajo, Thermophysical Properties of MOX and UO2 Fuels Including the Effects of Irradiation, Oak Ridge National Laboratory, 2000.
[27] J.H. Lienhard, On the commonality of equations for natural convection from immersed bodies, Int. J. Heat Mass Tran. 16 (11) (1973) 2121–2123.
[28] KAERI, MARS Code Manual Volume I - Code Structure, System Models and Solution Methods, 2006. Daejeon, Korea.
[29] Y.-H. Shin, J. Cho, J. Lee, H. Ju, S. Sohn, Y. Kim, H. Noh, I.S. Hwang, Experimental studies and computational benchmark on heavy liquid metal natural circulation in a full height-scale test loop for small modular reactors, Nucl. Eng. Des. 316 (2017) 26–37.
[30] J.H. Cho, A. Batta, V. Casamassima, X. Cheng, Y.J. Choi, I.S. Hwang, J. Lim, P. Meloni, F.S. Nitti, V. Dedul, et al., Benchmarking of thermal hydraulic loop models for Lead-Alloy Cooled Advanced Nuclear Energy System (LACANES), phase-I: isothermal steady state forced convection, J. Nucl. Mater. 415 (3) (2011) 404–414.
[31] F.W. Dittus, L.M.K. Boelter, Heat Transfer in Automobile Radiators of the Tubular Type, vol. 2, University of California publications in Engineering, 1930, pp. 443–461.